ACS OMEGA

Open Access

http://pubs.acs.org/journal/acsodf

Article

An Integrated Neural Optrode with Modification of Polymer-Carbon Composite Films for Suppression of the Photoelectric Artifacts

Yanyan Xu, Xien Yang, Zhiwen Liang, Lizhang Lin, Wenbo Zhao, Liyang Wang, Yu Xia, Xudong Lin, Mang I. Vai, Sio Hang Pun, and Baijun Zhang*

Cite This: *ACS Omega* 2024, 9, 33119−33129

Read Online

ACCESS | Metrics & More | Article Recommendations | Supporting Information

ABSTRACT: Optogenetics-based integrated photoelectrodes with high spatiotemporal resolution play an important role in studying complex neural activities. However, the photostimulation artifacts caused by the high level of integration and the high impedance of metal recording electrodes still hinder the application of photoelectrodes for optogenetic studies of neural circuits. In this study, a neural optrode fabricated on sapphire GaN material was proposed, and 4 μLEDs and 14 recording microelectrodes were monolithically integrated on a shank. Poly(3,4-ethylenedioxythiophene)/polystyrenesulfonate and multiwalled carbon nanotubes (PEDOT:PSS-MWCNT) and poly(3,4-ethylenedioxythiophene) and graphene oxide (PEDOT-GO) composite films were deposited on the surface of the recording microelectrode by electrochemical deposition. The results demonstrate that compared with the gold microelectrode, the impedances of both composite films reduced by more than 98%, and the noise amplitudes decreased by 70.73 and 87.15%, respectively, when exposed to light stimulation. Adjusting the high and low levels, we further reduced the noise amplitude by 48.3%. These results indicate that modifying the electrode surface by a polymer composite film can effectively enhance the performance of the microelectrode and further promote the application of the optrode in the field of neuroscience.

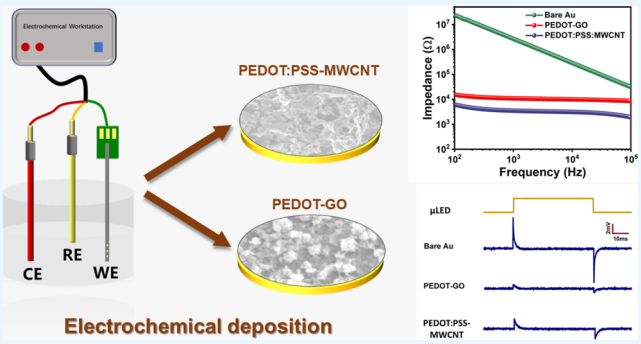

INTRODUCTION

In recent years, tremendous advances in neural interfaces have led researchers to better understand the brain's complex neural networks. These advancements have significantly propelled neuroscience research and the treatment of neurological disorders. Optogenetics-based neuromodulation tools are key to the study of neuroscience, which can regulate specific neurons expressing photosensitive proteins through light stimulation and record neuronal responses electrophysiologically with high spatiotemporal resolution. Since the concept of optogenetics was proposed, many researchers have introduced optogenetic tools with different structures for neuroscience research over the past few decades.[1−8] The traditional light source coupling optrode, that is, the laser or high-power light-emitting diode (LED) is coupled with the optical fiber as the light source, and the metal wires are used as the recording electrode, or alternatively, an external light source is coupled with the waveguide on a silicon-based substrate.[9−12] While this kind of optrode has little damage to the animal brain area, and it relies on an external light source, which will limit the range of animal activity. With the development of semiconductor materials and their processes, integrated LED optrodes have emerged, combining light sources and recording electrodes through semiconductor processes.[13−17] In 2015, Wu et al. first proposed the concept of fabrication of an integrated four-shank silicon-based probe on a commercial wafer, with each probe containing 12 μLEDs and 32 recording microelectrodes.[18] The integrated optrode has a high level of integration and higher spatiotemporal resolution, but there are also some problems. In order to reduce the damage of tissue implantation, the size of the optrode tends to be miniaturized. The recording site also tends to be high-pass-quantified to reduce the geometric size of the recording microelectrode. Correspondingly, the impedance of the recording microelectrode will also increase, which can easily cause interference during neural signal acquisition.[19−24]

In general, the conductive material of most recording electrodes is predominantly metal, such as gold, iridium, etc.[25,26] They have strong corrosion resistance and good biocompatibility. However, the elastic modulus of these materials is higher than that of brain tissue,[27] which makes the interface between the microelectrode and brain tissue

Received: May 13, 2024
Revised: July 7, 2024
Accepted: July 11, 2024
Published: July 17, 2024

https://doi.org/10.1021/acsomega.4c04534
ACS Omega 2024, 9, 33119−33129

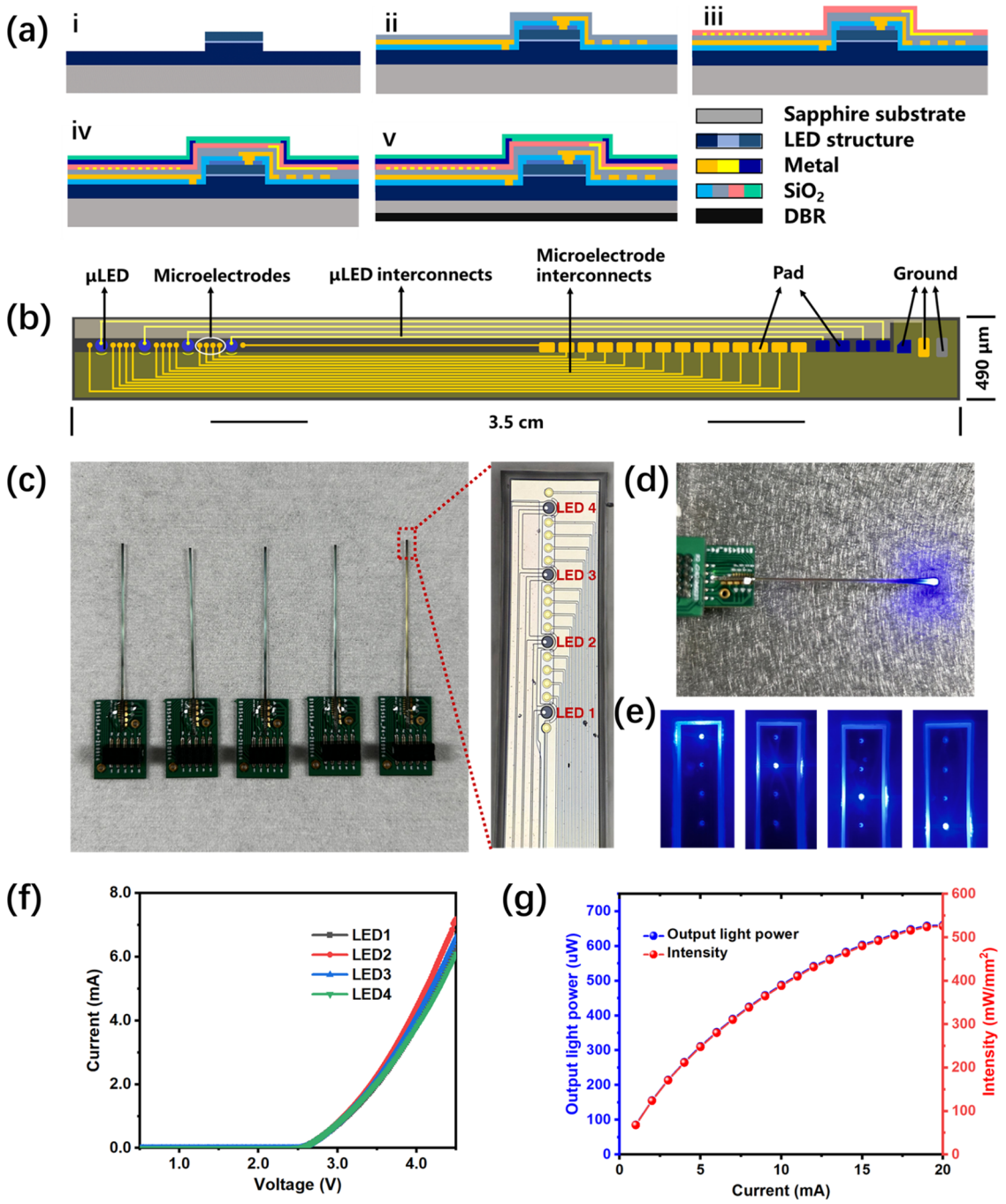

Figure 1. (a) Cross-sectional 2D schematic of the optoelectrode fabrication process. (i) Etching epitaxial layers to expose n-GaN layer; (ii) depositing the ohmic contact metal layer and passivation layer to form the μLED structure; (iii) depositing 1.5 μm Au as the microelectrodes; (iv) metal shielding layer; and (v) thinning the substrate backside and evaporating the DBR reflective layer. (b) Schematic diagram of the optrode structure. (c) Wire bonding the optoelectrode to the matching PCB; the red box shows the tip structure of optoelectrode. (d) Image of the optoelectrode during μLED operation. (e) Images of four μLED working, respectively. (f) $I-V$ curves of four μLEDs. (g) Output light power (blue) and intensity (red) of μLED.

produce stress mismatch. In addition, these metal microelectrodes usually have high impedance, which can reach several mega-ohms, and pose challenges to the subsequent circuitry of signal acquisition. These metal microelectrodes easily produce photoelectrochemical effect noise under light illumination, which is a common experiment scenario with optogenetic techniques.[28−30] These problems can restrict the application of electrodes in biological experiments. In order to improve the performance of microelectrodes, reduce impedance, and improve signal quality, researchers attempted to modify the electrode surface to improve the quality of microelectrodes, such as plating platinum black or iridium oxide.[31,32]

Regarding the surface modification technique on the microelectrode surface, conductive polymers have recently attracted much attention as materials for neural interfaces. PEDOT:PSS are among the most widely used conductive polymers, which have high conductivity properties, good

https://doi.org/10.1021/acsomega.4c04534
ACS Omega 2024, 9, 33119−33129

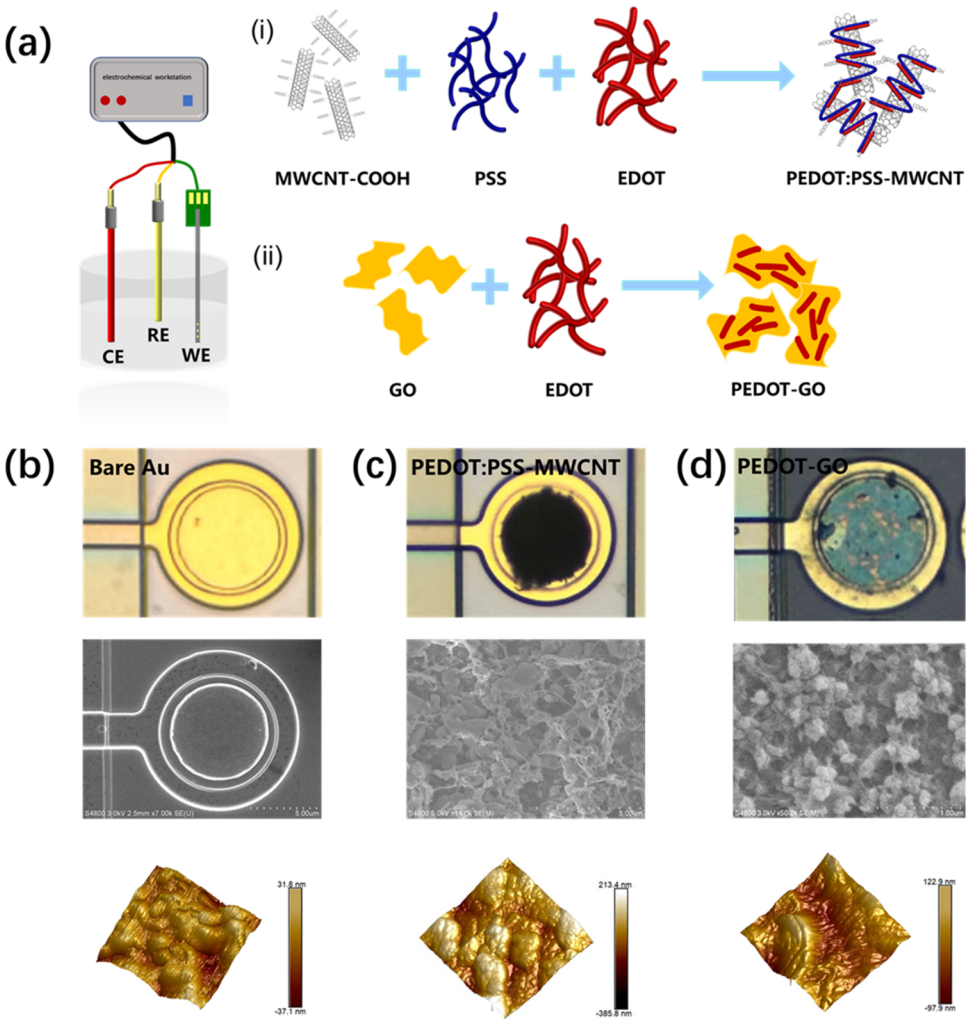

Figure 2. (a) Schematic diagram for the electrochemical deposition of PEDOT:PSS-MWCNT (i) and PEDOT:GO (ii) onto the microelectrode surface. Optical microscope images, scanning electron microscope images, and atomic force microscope images of (b) bare Au, (c) PEDOT:PSS-MWCNT, and (d) PEDOT:GO.

biocompatibility, adhesion, and stability.[33−35] Among them, PEDOT is the main one that plays a conductive role and its structure has conjugated double bonds. In addition, carbon materials, such as carbon nanotubes and graphene, are favored by researchers due to their high conductivity, high specific surface area, high mechanical strength, and low contact impedance. And many researchers have opted to combine them with polymer materials to modify the interfaces of recording microelectrodes.[35−40] In order to facilitate better bonding between carbon materials and polymers, many researchers subject the materials to acid treatment to enhance their functionality, and the functional groups carried on the surface can be better combined with the polymer material. This composite material can greatly increase the specific surface area of the microelectrode, effectively reduce the interfacial impedance, improve the adhesion of the composite film on the surface of the metal electrode, and improve the signal-to-noise ratio of nerve signals.[22,41,42]

In this article, we proposed a sapphire optrode with multiple drivers and multiple acquisition channels, which contains 4 μLEDs and 14 recording microelectrodes. To mitigate photostimulation artifacts, we designed a multimetal shielding layers architecture. Considering the influence of recording microelectrode size on impedance, we designed Au microelectrodes with diameters of 30, 40, and 50 μm and characterized the electrochemical properties of electrodes of different sizes. The results show that the larger the electrode size, the smaller the impedance is, which is conducive to reducing the noise interference generated when the signal is acquired. In addition, the PEDOT:PSS-MWCNT and PEDOT-GO films were deposited on the surface of the electrode by electrochemical deposition, respectively, resulting in a 98% reduction in impedance compared to the gold microelectrode, and the noise amplitude was reduced by 70.73 and 87.15%, respectively, after in vitro simulation experiments. It has been proven that the polymer-carbon composite film can effectively reduce the impedance of the recording electrode and improve its performance, thereby improving the signal-to-noise ratio of neural recording.

MATERIALS AND METHODS

Fabrication and Assembling of the Optrode. Figure 1a shows the fabrication steps of the sapphire optrode. First, the epitaxial layer was etched by inductively coupled plasma (ICP) to expose the n-type GaN layer to form the mesa structure of the LED. Then, a 1000 Å thickness layer of indium tin oxide (ITO) was deposited by magnetron sputtering, using photolithography and wet etching to retain a portion on the p-GaN

https://doi.org/10.1021/acsomega.4c04534
ACS Omega 2024, 9, 33119−33129

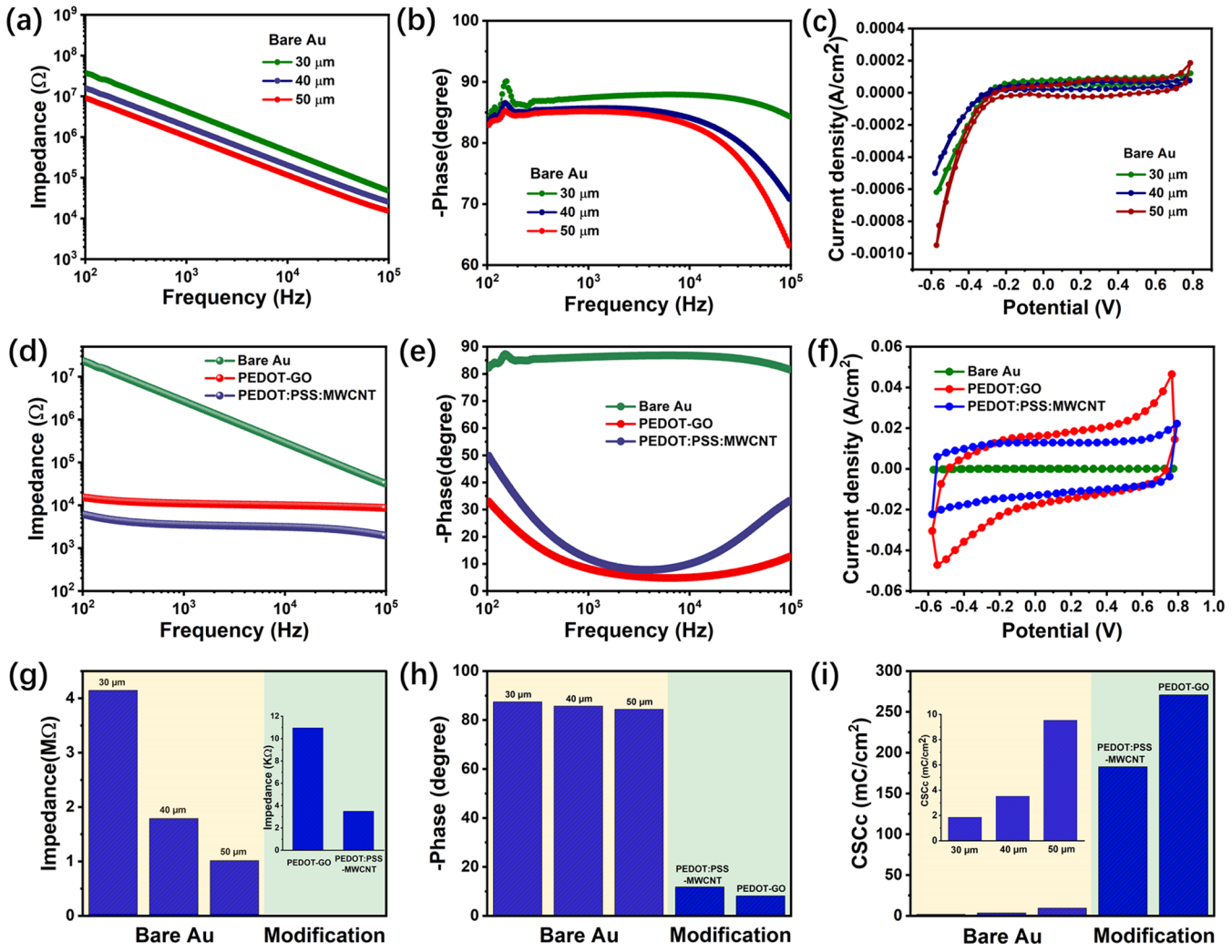

Figure 3. (a) Impedance spectra, (b) phase spectrum, and (c) cyclic voltammetry curves of bare Au microelectrodes with different sizes. (d) Impedance spectra, (e) phase spectrum, and (f) cyclic voltammetry curves of bare Au microelectrodes and modified microelectrodes with different materials (PEDOT-GO and PEDOT:PSS-MWCNT). Corresponding (g) impedance, (h) phase delay, and (i) CSCc values at 1 kHz.

layer to serve as the electrical contact layer, and rapidly annealing at 570 °C for 5 min; a 1 μm thick SiO_2 film was deposited through plasma enhanced chemical vapor deposition (PECVD) as an isolation layer at the sidewall of the insulated mesa; Cr/Ti metal was evaporated to form ohmic contacts with the n-GaN and p-GaN layers, followed by depositing another layer of SiO_2 film as a passivation layer. Next, 1.5 μm Au was evaporated to prepare microelectrodes and simultaneously prepare a metal shielding layer above the LED anode interconnects. After passivation with SiO_2, Cr/Ti metal was patterned as an additional shielding layer, followed by deposition of the final SiO_2 film. Windows were opened for all microelectrodes and bonding pads. Finally, the sapphire substrate was thinned to 150 μm. Then, a distributed Bragg reflector (DBR) was deposited on the back of the substrate. After laser scribing and cleaving, an independent optrode was obtained, with a length of 3.5 cm and a width of 490 μm, containing 4 μLEDs and 14 recording microelectrodes, as shown in Figure 1b. Subsequently, the optrodes are encapsulated. A single optrode was bonded to a matching PCB board using adhesive, and then an ultrasonic wire bonder was used to bond the optrode pads to the PCB board pads. To connect the external drive wires, the matching female headers were soldered to the PCB board by solder paste. Finally, the wire bonding locations were protected by photosensitive resin. The assembled optrode is shown in Figure 1c, and the red box shows an enlarged view of the tip of the optrode.

Optoelectrical Measurements. A semiconductor device parameter analyzer (Agilent B1500A, Keysight) measured the current−voltage (I−V) characteristics of μLEDs. An optical power meter (Newport 1919-R) was used to measure the output light power intensity of μLEDs with different currents.

Electrochemical Deposition. For this modification, 3,4-ethylene dioxy thiophene (EDOT) was obtained from Aladdin (China). Polystyrenesulfonate powder (PSS) was purchased from Macklin. The multiwalled carbon nanotube (MWCNT) with a 15 nm diameter and the graphene oxide (GO) dispersion were obtained from Tanfeng Tech. The electrochemical deposition experiments of the optrode were conducted on an electrochemical workstation (CS300, China) with a traditional three-electrode system; the Pt wire was the counter electrode (CE), the Ag/AgCl electrode was the reference electrode (RE), and the sapphire optrode was the working electrode (WE). The deposition device is shown in Figure 2a (left). The PEDOT:PSS-MWCNT is deposited using the following steps. First, 250 mg of PSS was added to 50

https://doi.org/10.1021/acsomega.4c04534
ACS Omega 2024, 9, 33119−33129

mL of deionized water, and ultrasonic dispersion made it completely dissolve; then, 50 mg of MWCNT was added to the solution and ultrasonically dispersed for 40 min. Second, an appropriate amount of EDOT solution was mixed into the dispersed solution, followed by 1.5 h of magnetic stirring to obtain the electrolyte solution. Then, the constant current was applied to deposit PEDOT:PSS-MWCNT with a current density of 0.2 mA/cm^2 in 10 min duration. The PEDOT:GO was deposited by using the following steps. First, 1 mg/mL GO solution was mixed into 50 mL of deionized water and ultrasonically dispersed for 30 min. Second, EDOT was added to the solution, followed by 1.5 h of magnetic stirring to obtain the electrolyte. Subsequently, the PEDOT:GO was deposited by a constant current with a current density of 0.2 mA/cm^2 in 10 min duration. Before depositing, the optrodes were pretreated by applying the cyclic voltammetry (CV) method with the potential range of −0.6 to 0.8 V for 10 cycles at a rate of 100 mV/s in the phosphate-buffered saline (PBS) solution.

Electrochemical Characterization. LCR meter (E4980A, KEYSIGHT) was applied to characterize the electrochemical impedance performances of the microelectrodes in the frequency range of 100 Hz and 1000 kHz via a 50 mV in standard PBS solution. The CV curves and stability were tested by the electrochemical workstation based on the three-electrode system. The CV scanning was performed at a scan potential range of −0.6 to 0.8 V, with a scan rate of 100 mV/s for 10 cycles in PBS solution.

Morphological Characterization. The surface morphologies of bare Au, PEDOT:PSS-MWCNT, and PEDOT-GO were imaged by scanning electron microscopy (SEM, S-4800). Photographs of atomic force microscopy (AFM) were taken on a Bruker Dimension Icon atomic force microscope by using the tapping mode.

In Vitro Measurement. The schematic diagram of the bench noise measurement system is described in Figure 5a. The assembled optrode was connected to the amplifier, and the tip of the optrode was immersed in PBS solution. A direct current power source (LPS-305) was used to drive the amplifier, and an oscilloscope (DSOX4024A, Keysight) was used to supply pulse signals to the μLED and record the noise signal.

RESULTS AND DISCUSSION

Optical Characterization of the Sapphire Optrode. We fabricated a sapphire optrode with 4 μLEDs and 14 recording microelectrodes on the shank, as shown in Figure 1c. The diameter of a single μLED is 60 μm, the actual light output area is 50 μm, and the vertical pitch between two adjacent μLEDs is 315 μm. The recording microelectrodes are available in different diameters, 30, 40, and 50 μm, respectively, and the pitch between two microelectrodes is 60 μm. Then, the electrical and optical properties of the μLED on the sapphire optrode were measured. Each LED on the shank can be activated individually, and Figure 1d,e shows the optical microscope images of μLEDs in different positions during operation. Figure 1f shows the $I-V$ curves of the four μLEDs. The corresponding rectified voltage curves are found to be basically consistent, confirming a turn-on voltage of 2.6 V. When the drive voltage is greater than 3.5 V, it can be found that there is a slight difference between the $I-V$ curves of the four μLEDs, which may be due to the different lead lengths and series resistors of the four μLEDs. Figure 1g shows the output light power and intensity of a representative μLED. It can be observed that it is easy to meet the requirement of the minimum power intensity of 1 mW/mm^2 to induce ChR2 activation with a small current.

Table 1. Impedance, Phase, and CSCc of Bare Au Microelectrode with Different Diameters

diameter (μm)	impedance (kΩ)	phase (deg)	CSCc (mC/cm^2)
30	4146.24 ± 149.95	−87.43 ± 0.16	1.86
40	1788.74 ± 48.3	−85.68 ± 0.32	3.52
50	1013.80 ± 63.34	−84.40 ± 1.18	9.54

Table 2. Impedance, Phase, and CSCc of Modified Microelectrodes

modification	impedance (kΩ)	phase (deg)	CSCc (mC/cm^2)
PEDOT:PSS-MWCNT	3.50 ± 0.17	−11.79 ± 0.63	182.74
PEDOT-GO	10.96 ± 2.29	−8.12 ± 1.67	270.74

Electrochemical Characterization of the Different-Size Au Microelectrodes. Different neurons have different sizes, and their diameters range from tens to hundreds of microns. In order to achieve a high spatial resolution recording and better analysis and measurement of neuronal activity, the size of the neural electrodes is designed to model the characteristic size of neurons. The advantages of this design are that the behavior of individual nerve cells can be recorded, and the density and diversity of electrodes on the probe can be increased.[43] Therefore, in the design of sapphire electrodes, we designed recording microelectrodes with diameters of 30, 40, and 50 μm, respectively. Electrochemical impedance spectroscopy is an important method for studying electrochemical performance at the microelectrode−electrolyte interface. The electrochemical characteristics of the recording microelectrodes with different diameters were detected in the frequency range from 100 Hz to 100 kHz. 1 kHz is the central frequency related to the neural activity. As shown in Figure 3a,b, the average impedances at 1 kHz are 4146.24 ± 149.95, 1788.74 ± 48.3, and 1013.8 ± 63.34 kΩ for the 30, 40, and 50 μm diameter microelectrodes (bare Au), respectively, the phases at 1 kHz are 87.43 ± 0.16, 85.68 ± 0.32, and 84.40 ± 1.18°. It can be seen from the results that impedance and phase decrease with increasing frequency, and the impedance decreases with increasing microelectrode geometric area, which indicates that the diffusion resistance and the double-layer capacitance decrease with the microelectrode diameter.[44] The charge storage capacity (CSC) is also one of the common parameters to evaluate the performance of the microelectrode. The enclosed area of the CV curves represents the CSC. The cathodal CSC (CSCc) value is often used to characterize the charge capacity of the microelectrode, which is the ratio of the integrated area of the cathode region of the CV curve to the area of the microelectrode.[39] After calculation, the CSCc values of 30, 40, and 50 μm are 1.86, 3.52, and 9.54 mC/cm^2, respectively. The electrochemical performance parameters of bare Au microelectrodes with different diameters are compared in Table 1. The result indicates that a large geometric area has lower impedance value and excellent charge storage capacity.

Electrochemical Characterization of Modified Microelectrodes. Increasing the geometric area of the metal recording microelectrode can effectively reduce the impedance,

https://doi.org/10.1021/acsomega.4c04534
ACS Omega 2024, 9, 33119−33129

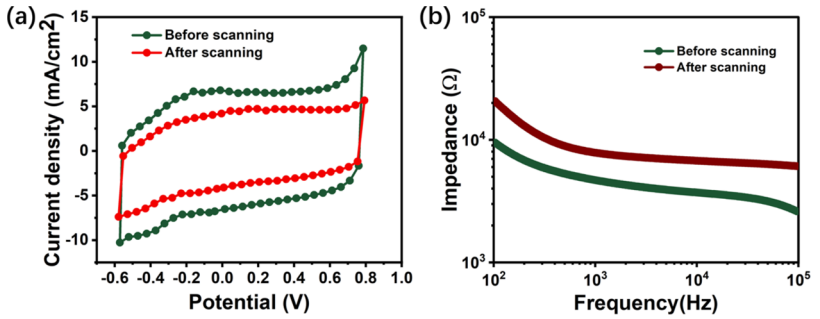

Figure 4. (a) Impedance and (b) cyclic voltammetry curves before and after 1000 cycles of PEDOT:PSS-MWCNT microelectrode.

but the microelectrode area cannot be increased indefinitely due to the limitation of the optrode size and practical biological application. It can also be seen from the above results that the microelectrode impedance is still several thousand kΩ after increasing the area. In addition, there is a mechanical mismatch between the metal microelectrode and the nerve tissue. The impedance suitable for the study of deep electrophysiological signals of brain tissue should be less than a few hundred kΩ; therefore, it is necessary to modify the surface of the microelectrode to reduce the impedance further and improve the recording performance of the optrode.

We selected a microelectrode with a diameter of 40 μm and chemically modified its surface by electrochemical deposition. PEDOT:PSS-MWCNT and PEDOT-GO will modify the microelectrode surface by electrochemical deposition, further reducing impedance and improving the recording properties. Figure 2a (i) shows the deposition process of the PEDOT:PSS-MWCNT. PSS acts as a counterion for PEDOT to be better dissolved in aqueous solutions. During the polymerization process, the EDOT monomer in solution is oxidized at the anode and positively charged, and then the oxidized EDOT polymerizes to form PEDOT. The functionalized MWCNT is negatively charged in the aqueous solution, which can balance the positive charge of PEDOT, and can be combined with PEDOT through $\pi-\pi$ conjugation to deposit together on the surface of the metal microelectrode, forming a high-performance polymer-carbon material composite film.[37] Figure 2a (ii) shows the deposition process of PEDOT-GO. The surface of graphene oxide (GO) contains a large number of hydroxyl (−OH) and carboxyl (−COOH) functional groups, which are negatively charged in aqueous solution, and can also serve as a binding site for graphene oxide to recombine with other polymers. In the electrochemical deposition process, the positively charged EDOT free radical interacts electrostatically with the negatively charged GO to form a PEDOT-GO composite film, which is deposited on the surface of the metal microelectrode.[45,46]

We compared the impedance, phase delay, and CSCc of bare Au, PEDOT:PSS-MWCNT, and PEDOT-GO, respectively. The results revealed that PEDOT:PSS-MWCNT and PEDOT-GO improved the impedance and phase performance. Figure 3d shows the impedance characteristics of both modified microelectrodes against the bare Au microelectrode. At 1 kHz, the average impedances are reduced from 4146.24 ± 149.95 to 3.5 ± 0.17 and 10.96 ± 2.29 kΩ, respectively, and that is decreased by 98% with respect to bare Au. The phase shifts at 1 kHz are changed from 87.43 ± 0.16 to 11.79 ± 0.63 and 8.12 ± 1.67°, as shown in Figure 3e. The results are also compared with those previously reported for the electrochemical properties of electrodes modified with different materials. Corresponding modification materials, values, and references are shown in Supporting Table S1. This suggests that both polymer composite films can effectively reduce the impedance, make the microelectrode less capacitive, and have a small phase delay. In addition, the method to evaluate CSCc of the microelectrode is CV characteritic. The CV curves, as plotted in Figure 3f, were tested, and the larger the enclosed area of the CV curve, the larger the charge storage capacity of the microelectrode. The results indicate that PEDOT-GO has a much larger encircled area than PEDOT:PSS-MWCNT and bare Au microelectrodes. By integrating the cathode portion of the CV curve and calculating it, the CSCc values of the PEDOT:PSS-MWCNT and PEDOT-GO microelectrodes are 182.74 and 270.74 mC/cm^2, respectively. The electrochemical performance parameters of the modified microelectrodes are shown in Table 2. Thus, the modifications of PEDOT:PSS-MWCNT and PEDOT-GO effectively reduce the impedance and improve the performance of recording microelectrode. The surface morphology of the microelectrodes before and after modification was also characterized. The optical images, SEM pictures, and three-dimensional (3D) AFM pictures of bare Au, PEDOT:PSS-MWCNT, and PEDOT-GO are depicted in Figure 2b−d. From the optical images, it can be seen that there are obvious depositions on the surface of microelectrodes compared to the bare Au. The SEM result shows that the PEDOT:PSS-MWCNT composites and the PEDOT-GO composites form rough and porous surfaces, which enlarge the electrochemical surface area and improve the performance of microelectrodes. In addition, AFM was used to characterize the surface morphology of bare Au and both modified microelectrodes. As depicted in Figure 2d, the surface roughness of microelectrodes coating PEDOT:PSS-MWCNT and PEDOT-GO is obviously changed compared to the bare Au. The surface roughness (R_q) values are 9.62, 60, and 32.84 nm, respectively, which were calculated from 2 μm × 2 μm scan range. The AFM results indicate that modified composite films have low impedance and minimum phase delay based on the larger surface area caused by rough structures.

Stability Measurements. The mechanical stability of PEDOT:PSS-MWCNT was measured in PBS solution by CV scanning on the modified microelectrode with a scan range from −0.6 to 0.8 V and a scan rate of 100 mV/s. Figure 4a shows the CV result after scanning 1000 cycles, in which the enclosed area of the CV curve decreased obviously. At the same time, the impedance after scanning was also measured. It can be seen from Figure 4b that the impedance at 1 kHz shows an obvious increase. The reason for this phenomenon may be that during the long-term scanning process, the conductive

https://doi.org/10.1021/acsomega.4c04534
ACS Omega 2024, 9, 33119−33129

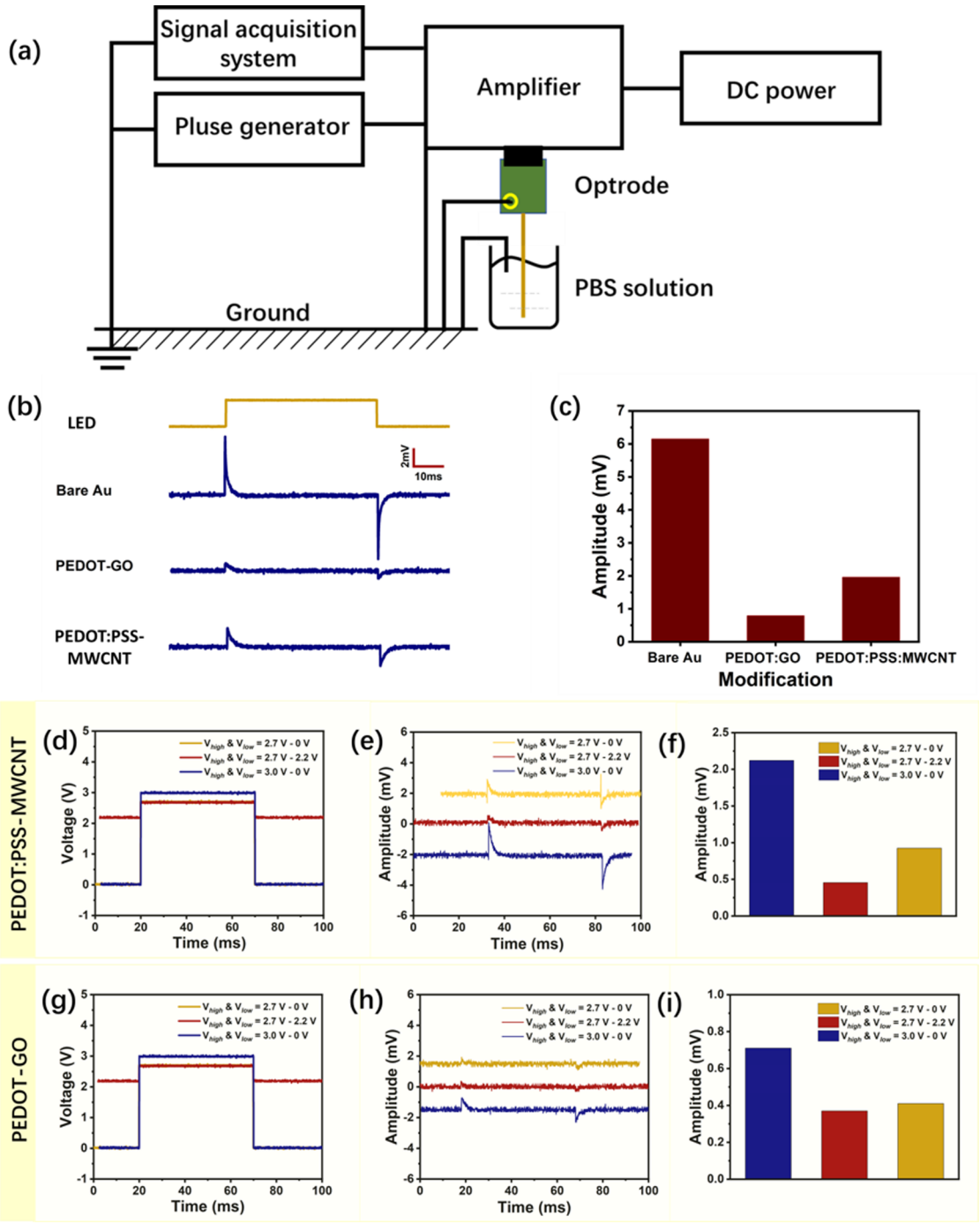

Figure 5. (a) Schematic diagram of the stimulation artifact tests; (b) stimulation artifact of bare Au, PEDOT-GO, and PEDOT:PSS-MWCNT microelectrodes under μLED working; and (c) corresponding amplitude values of microelectrodes with different materials. Adjusting the high-level voltage and low-level voltage to change the amplitudes of PEDOT:PSS-MWCNT- and PEDOT-GO-modified optrodes, where three different input pulse voltage signals are shown in (d, g); noise amplitudes with different pulse signals are shown in (e, h). (f, i) Corresponding histograms of positive amplitudes.

substances in the PEDOT:PSS-MWCNT film may be partially depleted due to electrochemical reactions, which hinders the electron transport and leads to an increase in impedance. At the same time, with the increase of scanning time, some conductive polymers in the film may undergo oxidation reactions due to long-term exposure to air, forming oxidized polymers that will affect the electrochemical properties of the film. In addition, the MWCNT in the film may be partially dedoped during long-term immersion and scanning, which hinders electron transmission inside the film and increases the impedance.

In Vitro Noise Tests. The noise of the optrode is mainly composed of two kinds: one is electromagnetic interference (EMI) caused by the active μLED and the equipment of the surroundings, and the other is photoelectric noise, which includes photoelectrochemical (PEC) noise caused by the metal microelectrode exposed to light and photovoltaic noise (PV) induced by the silicon substrate. In this work, the active

https://doi.org/10.1021/acsomega.4c04534
ACS Omega 2024, 9, 33119−33129

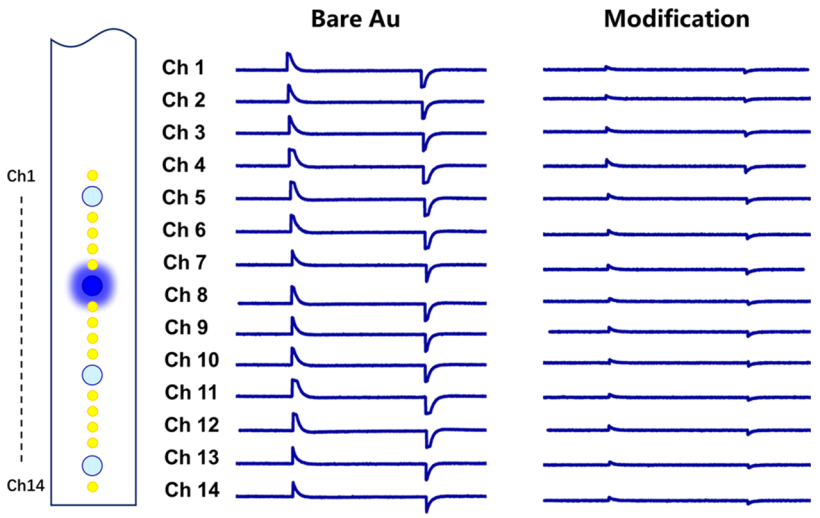

Figure 6. Waveforms recorded from the corresponding microelectrodes located in the different sites on the sapphire optrode. The bare Au microelectrodes and the PEDOT:PSS-MWCNT microelectrodes were compared. The pulse signal with a high level of 3.0 V and low level of 2.2 V, 10 Hz of frequency, 10 ms of duration, and 50% of duty cycle was applied to drive a single μLED.

optrode was fabricated on the GaN-on-sapphire so that the PV effect may be avoided, and the noise of the optrode could originate from the EMI and PEC. To quantify the amplitude of the photoelectric noises, the tip of the sapphire optrode was immersed in PBS solution (Figure 5a), and a square wave pulse was provided through the oscilloscope with an amplitude of 3.0 V, frequency of 10 Hz, and duty cycle of 50% was applied to turn on and off a single μLED. In order to reduce the EMI, multiple shielding layers were designed in the optrode structure. It is noted that the solution, amplifier, shielding layers, and optrode were cogrounded during the test process. As can be seen from Figure 5b, the noise amplitude of bare Au microelectrode is 6.5 mV. Although the shielding layers may suppress a part of the noise, the amplitude of residual noise is still large and is likely to derive from the PEC noise. Obviously, we can observe a significant decrease in the noise amplitudes of the microelectrodes after modification. The noise amplitudes of PEDOT:PSS-MWCNT and PEDOT-GO decreased to 1.80 and 0.79 mV, respectively. Compared with the bare Au, the amplitudes of modified microelectrodes decreased by 70.73 and 87.15%, respectively, as depicted in Figure 5c. The result shows that the amplitude noise decreases significantly after PEDOT:PSS-MWCNT and PEDOT-GO modifications, and the PEDOT-GO has the smallest noise amplitude. The reason that the amplitudes reduced after microelectrode modification is mainly attributed to the PEDOT:PSS-MWCNT and PEDOT-GO providing a rougher and porous surface, which have large specific surface areas and larger capacitances, and both composite materials can increase the conductivity of the microelectrode and reduce the impedance, thus improving the performance of the microelectrode.

In addition, we can further reduce the residual noise amplitude by adjusting the high and low pulse levels.[19,35,47] The experiment was carried out with the PEDOT:PSS-MWCNT and PEDOT-GO-modified microelectrode. As shown in Figure 5d–f about the test result of PEDOT:PSS-MWCNT microelectrode, when the low-level voltage is unchanged (0 V), the high-level voltage changes from 3 to 2.7 V, and the noise amplitude decreases from 1.80 to 0.93 mV by 48.33%, and when the high-level voltage is fixed at 2.7 V, the low-level voltage changes from 0 to 2.2 V (the value is lower than the μLED turn-on voltage), and the noise amplitude decreases to 0.57 mV by 38.71%. The PEDOT-GO modified optrode was tested under the same term, as depicted in Figure 5g–i. When the high-level voltage changes from 3 to 2.7 V, and the noise amplitude decreases from 0.79 to 0.42 mV by 46.8%, and when the high-level voltage is fixed at 2.7 V, the low-level voltage changes from 0 to 2.2 V, and the noise amplitude decreases to 0.38 mV. Moreover, the noise waveforms of Au microelectrodes and PEDOT:PSS-MWCNT microelectrodes recorded from all 14 sites are compared in Figure 6. The result indicates that the noises have a significant suppression, and the suppressed noise may mainly originate from the interference caused by the shielding defects. When the low voltage value remains constant, an increase in the high-level voltage leads to an increase in optical power, resulting in enhanced EMI and an increase in the noise amplitude. When the high voltage value is kept constant, increasing the low level close to the turn-on voltage threshold of the μLED results in the optical power remaining relatively steady while leading to a significant reduction in noise amplitude. This method changes the instantaneous voltage variable of the LED by adjusting the difference between the high and low voltage levels, also affecting the coupling capacitance between the recording traces, thereby causing a change in the noise amplitude.

CONCLUSIONS

This research proposes a sapphire optrode with a monolithic integration of four LEDs and 14 recording microelectrodes. A multilayer metal shield is designed in the structure to suppress electromagnetic interference caused by active LEDs and external environmental equipment. The influence of microelectrode size on impedance is verified, revealing a decrease in microelectrode impedance with increased electrode size, conducive to reducing noise amplitude. In addition, PEDOT:PSS-MWCNT and PEDOT-GO modifications are employed to improve the performance of the microelectrodes, and the results show that due to the large specific surface area and porous structure of the modified microelectrodes, the microelectrode obtains lower impedances and higher CSCc values. Moreover, in vitro simulation experiments confirm the effectiveness of the modified microelectrode in suppressing the

https://doi.org/10.1021/acsomega.4c04534
ACS Omega 2024, 9, 33119−33129

residual photoelectric noise. Further reduction of noise is achieved by adjusting the difference between the high and low levels of the LED pulse. In conclusion, the sapphire optrode, when modified with polymer-carbon composite films, presents the potential for optogenetic applications. In a future study, the optrode will be used for in vivo electrophysiological recording and photogenetic experiments. Based on the advantages of optrode with long shanks, high hardness, and multichannel optical stimulation and recording sites, it may have certain advantages in detecting neural activity in different areas of deep brain tissue.

■ ASSOCIATED CONTENT

Supporting Information

The Supporting Information is available free of charge at https://pubs.acs.org/doi/10.1021/acsomega.4c04534.

Performance comparison of microelectrodes modified with different materials (PDF)

■ AUTHOR INFORMATION

Corresponding Author

Baijun Zhang − *State Key Laboratory of Optoelectronic Materials and Technologies, School of Electronics and Information Technology, Sun Yat-Sen University, Guangzhou 510275, China*; Email: zhbaij@mail.sysu.edu.cn

Authors

Yanyan Xu − *State Key Laboratory of Optoelectronic Materials and Technologies, School of Electronics and Information Technology, Sun Yat-Sen University, Guangzhou 510275, China*; orcid.org/0000-0003-2621-3920

Xien Yang − *State Key Laboratory of Optoelectronic Materials and Technologies, School of Electronics and Information Technology, Sun Yat-Sen University, Guangzhou 510275, China*

Zhiwen Liang − *State Key Laboratory of Optoelectronic Materials and Technologies, School of Electronics and Information Technology, Sun Yat-Sen University, Guangzhou 510275, China*; orcid.org/0000-0003-2394-4947

Lizhang Lin − *State Key Laboratory of Optoelectronic Materials and Technologies, School of Electronics and Information Technology, Sun Yat-Sen University, Guangzhou 510275, China*

Wenbo Zhao − *State Key Laboratory of Optoelectronic Materials and Technologies, School of Electronics and Information Technology, Sun Yat-Sen University, Guangzhou 510275, China*

Liyang Wang − *State Key Laboratory of Analog and Mixed-Signal VLSI, Institute of Microelectronics, University of Macau, Macau 999078, China*

Yu Xia − *State Key Laboratory of Analog and Mixed-Signal VLSI, Institute of Microelectronics, University of Macau, Macau 999078, China*

Xudong Lin − *School of Biomedical Engineering, Sun Yat-Sen University, Guangzhou 510275, China*; orcid.org/0000-0001-5479-4414

Mang I. Vai − *State Key Laboratory of Analog and Mixed-Signal VLSI, Institute of Microelectronics, University of Macau, Macau 999078, China*

Sio Hang Pun − *State Key Laboratory of Analog and Mixed-Signal VLSI, Institute of Microelectronics, University of Macau, Macau 999078, China*

Complete contact information is available at: https://pubs.acs.org/10.1021/acsomega.4c04534

Author Contributions

Y.X. conceived this idea and designed the experiments. B.Z. supervised and directed this work. X.Y., Z.L., L.L., and W.Z. provided the experimental help. L.W. and Y.X. designed and provided the amplifier. X.L., I.V., and H.P. provided help in writing.

Notes

The authors declare no competing financial interest.

■ ACKNOWLEDGMENTS

This work was supported by the joint funding of the Nature Science Foundation of China (NSFC) and the Macao Science and Technology Development Fund (FDCT) of China (grant nos. 62061160368 and 0022/2020/AFJ).

■ REFERENCES

(1) Deisseroth, K. Optogenetics. *Nat. Methods* **2011**, *8* (1), 26−29.

(2) Boyden, E. S.; Zhang, F.; Bamberg, E.; Nagel, G.; Deisseroth, K. Millisecond-timescale, genetically targeted optical control of neural activity. *Nat. Neurosci.* **2005**, *8* (9), 1263−1268.

(3) Buchen, L. Neuroscience: Illuminating the brain. *Nature* **2010**, *465* (7294), 26−28.

(4) Shirai, F.; Hayashi-Takagi, A. Optogenetics: Applications in psychiatric research. *Psychiatry Clin. Neurosci.* **2017**, *71* (6), 363−372.

(5) Le, S.; Zhang, Y.; Fu, Y. F.; Fang, T.; Song, Z. T.; Zang, X. Z.; Zhan, G. G.; Wang, S. Y.; Li, H.; Tao, J.; Liang, J. Q.; Zhang, L. H.; Kang, X. Y. In *Implantable Optoelectronic Neural Interface for Optogenetics*, Implantable Optoelectronic Neural Interface for Optogenetics; IEEE, 2021; pp 241−246.

(6) Luo, J.; Xue, N.; Chen, J. A Review: Research Progress of Neural Probes for Brain Research and Brain−Computer Interface. *Biosensors* **2022**, *12* (12), No. 1167.

(7) Almasri, R. M.; Ladouceur, F.; Mawad, D.; Esrafilzadeh, D.; Firth, J.; Lehmann, T.; Poole-Warren, L. A.; Lovell, N. H.; Al Abed, A. Emerging trends in the development of flexible optrode arrays for electrophysiology. *APL Bioeng.* **2023**, *7* (3), No. 031503, DOI: 10.1063/5.0153753.

(8) Moorthy, V. M.; Varatharajan, P.; Rathnasami, J. D.; Srivastava, V. M. G-Optrode Bio-Interfaces for Non-Invasive Optical Cell Stimulation: Design and Evaluation. *Biosensors* **2022**, *12* (10), No. 808, DOI: 10.3390/bios12100808.

(9) Ryu, D.; Lee, Y.; Lee, Y.; Lee, Y.; Hwang, S.; Kim, Y. K.; Jun, S. B.; Lee, H. W.; Ji, C. H. Silicon optrode array with monolithically integrated SU-8 waveguide and single LED light source. *J. Neural Eng.* **2022**, *19* (4), No. 046013.

(10) Shin, H.; Son, Y.; Chae, U.; Kim, J.; Choi, N.; Lee, H. J.; Woo, J.; Cho, Y.; Yang, S. H.; Lee, C. J.; Cho, I. J. Multifunctional multi-shank neural probe for investigating and modulating long-range neural circuits in vivo. *Nat. Commun.* **2019**, *10* (1), No. 3777.

(11) Yu, J. X.; Ling, W.; Li, Y.; Ma, N.; Wu, Z. Y.; Liang, R.; Pan, H. Z.; Liu, W. T.; Fu, B.; Wang, K.; Li, C. X.; Wang, H. J.; Peng, H.; Ning, B. A.; Yang, J. J.; Huang, X. A Multichannel Flexible Optoelectronic Fiber Device for Distributed Implantable Neurological Stimulation and Monitoring. *Small* **2021**, *17* (4), No. 2005925.

(12) Wang, L. C.; Wang, M. H.; Ge, C. F.; Ji, B. W.; Guo, Z. J.; Wang, X. L.; Yang, B.; Li, C. Y.; Liu, J. Q. The use of a double-layer platinum black-conducting polymer coating for improvement of neural recording and mitigation of photoelectric artifact. *Biosens. Bioelectron.* **2019**, *145*, No. 111661.

(13) Kim, K.; Wu, F.; Wise, K. D.; Yoon, E. GaN-on-Silicon MicroLEDs for Neural Interfaces. *Semiconductors and Semimetals*; Elsevier, 2021; *106*, pp 123−172.

(14) McAlinden, N.; Gu, E.; Dawson, M. D.; Sakata, S.; Mathieson, K. Optogenetic activation of neocortical neurons in vivo with a

sapphire-based micro-scale LED probe. *Front. Neural Circuits* **2015**, *9*, No. 25.
(15) Scharf, R.; Tsunematsu, T.; McAlinden, N.; Dawson, M. D.; Sakata, S.; Mathieson, K. Depth-specific optogenetic control in vivo with a scalable, high-density μLED neural probe. *Sci. Rep.* **2016**, *6* (1), No. 28381.
(16) McAlinden, N.; Reiche, C. F.; Clark, A. M.; Scharf, R.; Cheng, Y.; Sharma, R.; Rieth, L.; Dawson, M. D.; Angelucci, A.; Mathieson, K.; Blair, S. In vivo optogenetics using a Utah Optrode Array with enhanced light output and spatial selectivity *bioRxiv* 2024, DOI: 10.1101/2024.03.18.585479.
(17) Kampasi, K.; English, D. F.; Seymour, J.; Stark, E.; McKenzie, S.; Voroslakos, M.; Buzsaki, G.; Wise, K. D.; Yoon, E. Dual color optogenetic control of neural populations using low-noise, multishank optoelectrodes. *Microsyst. Nanoeng.* **2018**, *4*, No. 10.
(18) Wu, F.; Stark, E.; Ku, P.-C.; Wise, K. D.; Buzsáki, G.; Yoon, E. Monolithically Integrated μLEDs on Silicon Neural Probes for High-Resolution Optogenetic Studies in Behaving Animals. *Neuron* **2015**, *88* (6), 1136−1148.
(19) Kim, K.; Vöröslakos, M.; Seymour, J. P.; Wise, K. D.; Buzsáki, G.; Yoon, E. Artifact-free and high-temporal-resolution in vivo opto-electrophysiology with microLED optoelectrodes. *Nat. Commun.* **2020**, *11* (1), No. 2063.
(20) Yasunaga, H.; Takagi, T.; Shinko, D.; Nakayama, Y.; Takeuchi, Y.; Nishikawa, A.; Loesing, A.; Ohsawa, M.; Sekiguchi, H. Development of a neural probe integrated with high-efficiency MicroLEDs for in vivo application. *Jpn. J. Appl. Phys.* **2021**, *60* (1), No. 016503.
(21) Vöröslakos, M.; Kim, K.; Slager, N.; Ko, E.; Oh, S.; Parizi, S. S.; Hendrix, B.; Seymour, J. P.; Wise, K. D.; Buzsáki, G.; Fernández-Ruiz, A.; Yoon, E. HectoSTAR μLED Optoelectrodes for Large-Scale, High-Precision In Vivo Opto-Electrophysiology. *Adv. Sci.* **2022**, *9* (18), No. 2105414.
(22) Zeng, Q.; Huang, Z. L. Challenges and Opportunities of Implantable Neural Interfaces: From Material, Electrochemical and Biological Perspectives. *Adv. Funct. Mater.* **2023**, *33* (32), No. 2301223.
(23) Goncalves, S. B.; Palha, J. M.; Fernandes, H. C.; Souto, M. R.; Pimenta, S.; Dong, T.; Yang, Z.; Ribeiro, J. F.; Correia, J. H. LED Optrode with Integrated Temperature Sensing for Optogenetics. *Micromachines* **2018**, *9* (9), No. 473, DOI: 10.3390/mi9090473.
(24) Xu, Y.; Xia, N.; Lim, X.; Tran, M. H.; Boulger, E.; et al. Multichannel optrodes for photonic stimulation. *Neurophotonics* **2018**, *5* (04), No. 045002, DOI: 10.1117/1.nph.5.4.045002.
(25) della Valle, E.; Welle, E. J.; Chestek, C. A.; Weiland, J. D. Compositional and morphological properties of platinum-iridium electrodeposited on carbon fiber microelectrodes. *J. Neural Eng.* **2021**, *18* (5), No. 054001.
(26) Shen, J. Y.; Xu, Y. Y.; Xiao, Z. W.; Liu, Y. B.; Liu, H. H.; Wang, F. G.; Yao, W. Q.; Yan, Z. K.; Zhang, M. J.; Wu, Z. S.; Liu, Y.; Pun, S. H.; Lei, T. C.; Vai, M. I.; Mak, P. U.; Chen, C. H.; Zhang, B. J. Influence of the Surface Material and Illumination upon the Performance of a Microelectrode/Electrolyte Interface in Optogenetics. *Micromachines* **2021**, *12* (9), No. 1061.
(27) Lacour, S. P.; Courtine, G.; Guck, J. Materials and technologies for soft implantable neuroprostheses. *Nat. Rev. Mater.* **2016**, *1* (10), No. 16063.
(28) Han, X. In Vivo Application of Optogenetics for Neural Circuit Analysis. *ACS Chem. Neurosci.* **2012**, *3* (8), 577−584.
(29) Cho, Y. U.; Lee, J. Y.; Jeong, U. J.; Park, S. H.; Lim, S. L.; Kim, K. Y.; Jang, J. W.; Park, J. H.; Kim, H. W.; Shin, H.; Jeon, H.; Jung, Y. M.; Cho, I. J.; Yu, K. J. Ultra-Low Cost, Facile Fabrication of Transparent Neural Electrode Array for Electrocorticography with Photoelectric Artifact-Free Optogenetics. *Adv. Funct. Mater.* **2021**, *32* (10), No. 2105568.
(30) Wang, M. H.; Fan, Y.; Li, L. L.; Wen, F.; Guo, B. B.; Jin, M. Y.; Xu, J. H.; Zhou, Y. H.; Kang, X. Y.; Ji, B. W.; Cheng, Y. H.; Wang, G. F. Flexible Neural Probes with Optical Artifact-Suppressing Modification and Biofriendly Polypeptide Coating. *Micromachines* **2022**, *13* (2), No. 199.
(31) Boehler, C.; Oberueber, F.; Schlabach, S.; Stieglitz, T.; Asplund, M. Long-Term Stable Adhesion for Conducting Polymers in Biomedical Applications: IrOx and Nanostructured Platinum Solve the Chronic Challenge. *ACS Appl. Mater. Interfaces* **2017**, *9* (1), 189−197.
(32) Ji, B.; Ge, C.; Guo, Z.; Wang, L.; Wang, M.; Xie, Z.; Xu, Y.; Li, H.; Yang, B.; Wang, X.; Li, C.; Liu, J. Flexible and stretchable optoelectric neural interface for low-noise electrocorticogram recordings and neuromodulation in vivo. *Biosens. Bioelectron.* **2020**, *153*, No. 112009.
(33) Fan, X.; Nie, W. Y.; Tsai, S. H.; Wang, N. X.; Huang, H. H.; Cheng, Y. J.; Wen, R. J.; Ma, L. J.; Yan, F.; Xia, Y. G. PEDOT:PSS for Flexible and Stretchable Electronics: Modifications, Strategies, and Applications. *Adv. Sci.* **2019**, *6* (19), No. 1900813.
(34) Kayser, L. V.; Lipomi, D. J. Stretchable Conductive Polymers and Composites Based on PEDOT and PEDOT:PSS. *Adv. Mater.* **2019**, *31* (10), No. 1806133.
(35) Mao, D. C.; Sun, F.; Driscoll, B.; Li, Z. H.; Xu, G. Y. Close-packed dual-color micro-LEDs enable cortical-layer-specific bidirectional in vivo optogenetic electrophysiology. *Cell Rep. Phys. Sci.* **2023**, *4* (12), No. 101702.
(36) Saunier, V.; Flahaut, E.; Blatché, M. C.; Bergaud, C.; Maziz, A. Carbon nanofiber-PEDOT composite films as novel microelectrode for neural interfaces and biosensing. *Biosens. Bioelectron.* **2020**, *165*, No. 112413.
(37) Lu, Z. Y.; Xu, S. W.; Wang, H.; He, E. H.; Liu, J. T.; Dai, Y. C.; Xie, J. Y.; Song, Y. L.; Wang, Y.; Wang, Y. D.; Qu, L. N.; Cai, X. X. PtNPt/MWCNT-PEDOT:PSS-Modified Microelectrode Arrays for the Synchronous Dopamine and Neural Spike Detection in Rat Models of Sleep Deprivation. *ACS Appl. Bio Mater.* **2021**, *4* (6), 4872−4884.
(38) Wang, M.; Guo, B.; Ji, B.; Fan, Y.; Wang, L.; Ye, L.; Chen, Y.; Cheng, Y.; Dong, L.; Wang, G. Controlled Electrodeposition of Graphene Oxide Doped Conductive Polymer on Microelectrodes for Low-Noise Optogenetics. *IEEE Electron Device Lett.* **2021**, *42* (3), 418−421.
(39) Xu, S.; Deng, Y.; Luo, J.; He, E.; Liu, Y.; Zhang, K.; Yang, Y.; Xu, S.; Sha, L.; Song, Y.; Xu, Q.; Cai, X. High-Throughput PEDOT:PSS/PtNPs-Modified Microelectrode Array for Simultaneous Recording and Stimulation of Hippocampal Neuronal Networks in Gradual Learning Process. *ACS Appl. Mater. Interfaces* **2022**, *14* (13), 15736−15746.
(40) Park, D.-W.; Schendel, A. A.; Mikael, S.; Brodnick, S. K.; Richner, T. J.; Ness, J. P.; Hayat, M. R.; Atry, F.; Frye, S. T.; Pashaie, R.; Thongpang, S.; Ma, Z.; Williams, J. C. Graphene-based carbon-layered electrode array technology for neural imaging and optogenetic applications. *Nat. Commun.* **2014**, *5* (1), No. 5258.
(41) Liu, R.; Feng, Z.-Y.; Li, D.; Jin, B.; Lan, Y.; Meng, L.-Y. Recent trends in carbon-based microelectrodes as electrochemical sensors for neurotransmitter detection: A review. *TrAC, Trends Anal. Chem.* **2022**, *148*, No. 116541.
(42) Vajrala, V. S.; Saunier, V.; Nowak, L. G.; Flahaut, E.; Bergaud, C.; Maziz, A. Nanofibrous PEDOT-Carbon Composite on Flexible Probes for Soft Neural Interfacing. *Front. Bioeng. Biotechnol.* **2021**, *9*, No. 780197.
(43) Woods, G. A.; Rommelfanger, N. J.; Hong, G. S. Bioinspired Materials for Bioelectronic Neural Interfaces. *Matter* **2020**, *3* (4), 1087−1113.
(44) Vatsyayan, R.; Dayeh, S. A. A universal model of electrochemical safety limits in vivo for electrophysiological stimulation. *Front. Neurosci.* **2022**, *16*, No. 972252.
(45) Deng, M.; Yang, X.; Silke, M.; Qiu, W.; Xu, M.; Borghs, G.; Chen, H. Electrochemical deposition of polypyrrole/graphene oxide composite on microelectrodes towards tuning the electrochemical properties of neural probes. *Sens. Actuators, B* **2011**, *158* (1), 176−184.
(46) Azman, N. H. N.; Lim, H. N.; Sulaiman, Y. Effect of electropolymerization potential on the preparation of PEDOT/

graphene oxide hybrid material for supercapacitor application. *Electrochim. Acta* **2016**, *188*, 785−792.
(47) Shen, J.; Xu, Y.; Xiao, Z.; Liu, Y.; Liu, H.; Wang, F.; Yan, C.; Wang, L.; Chen, C.; Wu, Z.; Liu, Y.; Mak, P. U.; Vai, M. I.; Pun, S. H.; Lei, T. C.; Zhang, B. Double-Sided Sapphire Optrodes with Conductive Shielding Layers to Reduce Optogenetic Stimulation Artifacts. *Micromachines* **2022**, *13* (11), No. 1836.

https://doi.org/10.1021/acsomega.4c04534
ACS Omega 2024, 9, 33119−33129